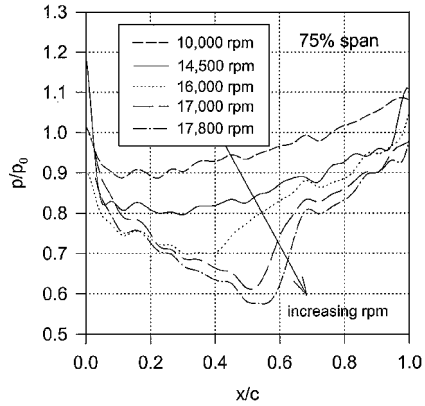

Fig. 3 PSP pressure distributions at 75% span.

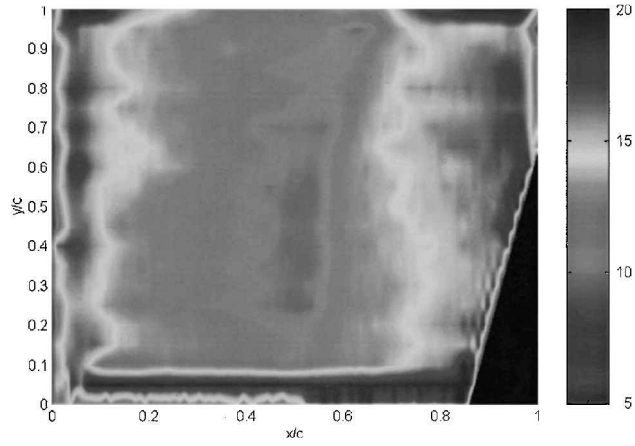

Fig. 4 Suction surface-pressure map at 17,500 rpm.

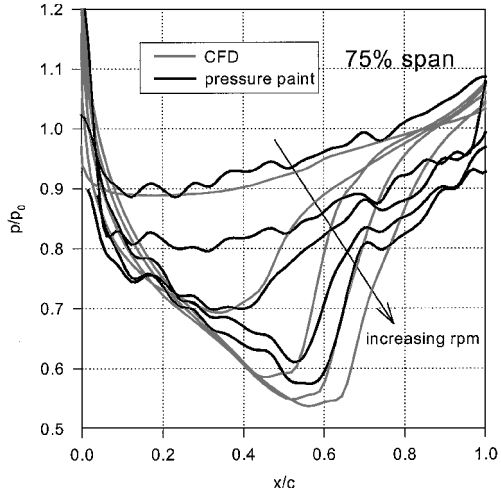

Fig. 5 Comparison between CFD results and PSP data at 75% span 10,000; 14,750; 16,000; 17,000; and 17,800 rpm.

Figure 3 shows a surface-pressure map at 17,800 rpm. This two-dimensional maps clearly indicate the formation of a shock that produces a rapid pressure rise across it Fig. 4. The black patch at the right edge results from blade overlap near the root.

A cascade analysis was performed at the 0.75 span of the rotor blade using Rotor Viscous Code Quasi-3D from R. Chima at NASA Lewis Research Center.[5] This Navier–Stokes code incorporates a Baldwin–Lomax turbulence model. Figure 5 shows comparison between computational fluid dynamics (CFD) results and PSP data at 75% span for different rotational speeds. The PSP-derived pressure distributions exhibit the same trend as those given by the CFD code. Quantitatively, the measured pressure data are lower than the CFD results.

Conclusions

Pressure- and temperature-sensitive paints have been used for the measurement of blade surface-pressure and temperature distributions in a high-speed axial compressor environment. Measurements of the suction surface pressure were made from the hub to tip in several rotational speeds. The two-dimensional surface pressure maps clearly indicate the presence of a shock wave at higher rotational speeds, which is not evident in the corresponding temperature maps.

References

[1]Johnston, R. T., and Fleeter, S., "Time Resolved Variations of an IGV Flow Field in the Presence of a Rotor Potential Field," AIAA Paper 96-2670, July 1996.

[2]Lui, T., Torgerson, S., Johnston, R., Fleeter, S., and Sullivan, J., "Rotor Blade Pressure Measurement in a High Speed Axial Compressor Using Pressure and Temperature Sensitive Paints," AIAA Paper 97-0162, Jan. 1997.

[3]Torgerson, S. D., "A Laser Scanning System for Use with Pressure and Temperature Sensitive Paints," Master's Thesis, School of Aeronautics and Astronautics, Purdue Univ., West Lafayette, IN, Aug. 1997.

[4]McLachlan, B. G., Kavandi, J. L., Callis, J. B., Gouterman, M., Green, E., and Khalil, G., "Surface Pressure Field Mapping Using Luminescent Coatings," *Experiments in Fluids*, Vol. 14, 1993, pp. 33–41.

[5]Chima, R. V., "Explicit Multigrid Algorithm for Quasi-Three-Dimensional Viscous Flows in Turbomachinery," *Journal of Propulsion and Power*, Vol. 3, No. 5, 1987, pp. 397–405.

Unsteady Flow in a Supersonic Turbine with Variable Specific Heats

Daniel J. Dorney* and Lisa W. Griffin†
NASA Marshall Space Flight Center,
Marshall Space Flight Center, Alabama 35812
Frank Huber‡
Riverbend Design Services, Palm Beach Gardens, Florida 33418
and
Douglas L. Sondak§
Boston University, Boston, Massachusetts 02215

Introduction

MODERN high-work turbines can be compact, transonic, supersonic, counter-rotating, or use a dense drive gas. The vast majority of modern rocket turbine designs fall into these categories. These turbines usually have large temperature variations across a given stage and are characterized by large amounts of flow unsteadiness. The flow unsteadiness can have a major impact on the turbine performance and durability. For example, the space transportation main engine fuel turbine, a high-work, transonic design, was found to have an unsteady interrow shock that reduced efficiency by two

Received 15 June 2001; revision received 16 September 2001; accepted for publication 2 October 2001.

*Aerospace Engineer, Applied Fluids Dynamic Analysis Branch. Senior Member AIAA.

†Team Leader, Applied Fluids Dynamic Analysis Branch. Senior Member AIAA.

‡President. Senior Member AIAA.

§Senior Scientific Programmer, Office of Information Technology. Senior Member AIAA.

points and increased dynamic loading by 24%. The revolutionary reusable technology turbopump (RRTT), which uses full flow oxygen for its drive gas, was found to shed vortices with such energy as to raise serious blade durability concerns. In both cases, the sources of the problems were uncovered (before turbopump testing) with the application of validated, unsteady computational fluid dynamics (CFD) to the designs. In the case of the RRTT and the alternate turbopump development turbines, the unsteady CFD codes have been used not just to identify problems, but to guide designs that mitigate problems due to unsteadiness. Using unsteady flow analyses as a part of the design process has led to turbine designs with higher performance (which affects temperature and mass flow rate) and fewer dynamics problems. The works of Griffin et al.,[1] Garcia et al.,[2] and Griffin and Dorney,[3] are examples of the application of unsteady CFD to rocket turbine designs.

One of the many assumptions made during the design and analysis of supersonic turbine stages is that the values of the specific heats are constant. In some analyses the value is based on an average of the expected upstream and downstream temperatures. In stages where the temperature can vary by 300–500 K, however, the assumption of constant fluid properties may lead to erroneous performance and durability predictions. In this study the suitability of assuming constant specific heats has been investigated by performing three-dimensional unsteady Navier–Stokes simulations for a supersonic turbine stage. In the first simulation the fluid properties were held constant, whereas in the second simulation the specific heats were allowed to vary locally as a function of static temperature. The predicted results from both simulations have been compared to the results of a well-validated meanline analysis that was also modified for variable specific heats. The meanline analysis is composed of one-dimensional equations of motion and empirical correlations.

Numerical Algorithm

The governing equations considered in this study are the time-dependent, three-dimensional, Reynolds-averaged Navier–Stokes equations. To extend the equations of motion to turbulent flows, an eddy viscosity formulation is used. The turbulent viscosity is calculated using a two-layer algebraic turbulence model. The numerical algorithm consists of a time-marching, implicit, finite difference scheme. The procedure is third-order spatially accurate and second-order temporally accurate. The inviscid fluxes are discretized using a third-order upwind-biased scheme, whereas the viscous fluxes are calculated using standard central differences. An approximate-factorization technique is used to compute the time rate changes in the conserved variables. The numerical analysis uses message passing interface to reduce the computation time for large-scale three-dimensional simulations.

The Navier–Stokes analysis uses O- and H-type zonal grids to discretize the flowfield and facilitate relative motion of the rotating components. The O-grids are body fitted to the surfaces of the airfoils and generated using an elliptic equation solution procedure. They are used to resolve properly the viscous flow in the blade passages and to apply easily the algebraic turbulence model. The algebraically generated H-grids are used to discretize the remainder of the flowfield.

The computational analysis has been validated on several supersonic turbine geometries (for example, in Refs. 3 and 4).

Geometry and Grids

The supersonic turbine configuration, typical of those proposed for a reusable launch vehicle, consists of 21 vane airfoils and 52 rotor blades. In the current effort, a two-vane/five-rotor blade count approximation has been made. To keep the pitch-to-chord ratio constant, the vane airfoils were scaled by factor of $\frac{21}{20}$ and the rotor blades were scaled by a factor of $\frac{52}{50}$. The rotor tip clearance was set at a typical value of approximately 2.5% of the rotor height. Two simulations have been performed for the turbine, one with constant specific heats (case 1) and one in which the specific heats vary as a function of temperature (case 2).

The grid dimensions (number of passages $\times\, i \times j \times k$) for the turbine simulations are presented in Table 1. Previous simulations

Table 1 Computational grid dimensions

Grid type	Vane	Rotor
O	$2 \times 121 \times 31 \times 38$	$5 \times 121 \times 21 \times 38$
H	$2 \times 86 \times 41 \times 38$	$5 \times 82 \times 21 \times 38$
Tip	——	$5 \times 121 \times 16 \times 5$
Total points	553,052	858,370

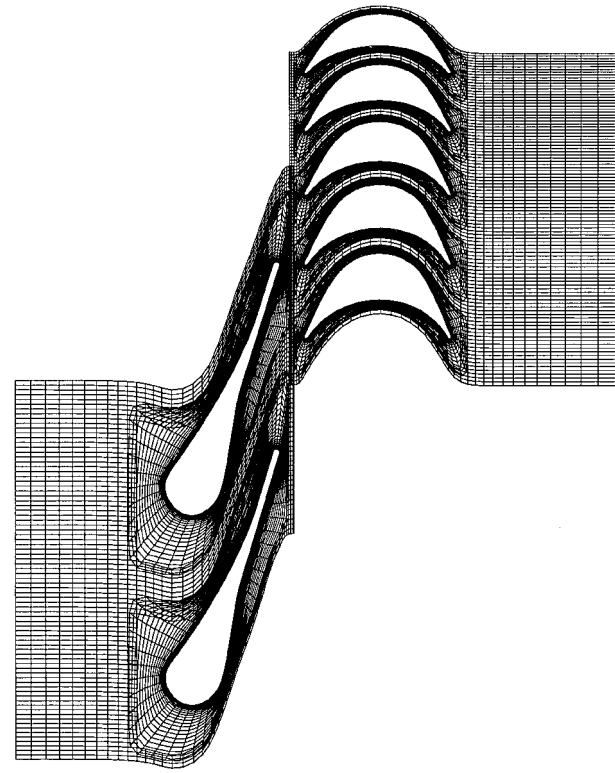

Fig. 1 Midspan section of turbine grid.

suggested that 38 spanwise planes are adequate to resolve the predominant flow features for this type of geometry.[3] Figure 1 illustrates the midspan section of the computational grids. The total number of grid points used to discretize the turbine was 1,363,022. The average value of y^+, the nondimensional distance of the first grid line above the surface, was approximately 1.5 for the airfoil surfaces and 3.5 for the endwalls.

The simulations were run on seven 250-MHz processors of an SGI Origin2000. Each simulation was run for 12.5 global cycles (in excess of one complete rotor revolution) at 25,000 iterations per cycle, where a global cycle is defined as the time it takes for the five rotor blades to pass the two vane airfoils. The value of 25,000 iterations per cycle was chosen to resolve all of the expected frequencies of interest. Each iteration required approximately 16 s computation time on seven processors. The time periodicity of the solutions was determined by plotting pressure traces at different points along the airfoil surfaces.

Numerical Results

The turbine under consideration has an inlet Mach number of $M_0 = 0.12$, an inlet static pressure of 15.2 MPa, and an inlet static temperature of $T_0 = 1232$ K. The rotor rotates at $\Omega = 31,300$ rpm, the Reynolds number (based on the inlet conditions and the rotor axial chord) is approximately 5×10^5, and the ratio of the rotor exit static pressure to vane inlet total pressure is $P_2/P_{t0} = 0.1875$. The operating fluid in the turbine is a gaseous hydrogen mixture. In case 1 a constant specific heat ratio of $\gamma = 1.354$ was assumed, whereas in case 2 the specific heat ratio was varied locally according to the following equations:

$$\gamma = \frac{C_p/R}{(C_p/R) - 1} \tag{1}$$

$$\frac{C_p}{R} = a_1 + a_2 \times T + a_3 \times T^2 + a_4 \times T^3 + a_5 \times T^4 \qquad (2)$$

where the coefficients for hydrogen are[5]:

$$a_1 = 0.39508691E{+}01, \qquad a_2 = 0.10207987E{+}00$$
$$a_3 = 0.13124466E{-}04, \qquad a_4 = -0.76649284E{-}07$$
$$a_5 = 0.34503763E{-}10$$

for temperatures between 300 and 1000 K, and

$$a_1 = 0.36440206E{+}02, \qquad a_2 = 0.54614801E{-}01$$
$$a_3 = -0.16091151E{-}04, \qquad a_4 = 0.21478497E{-}08$$
$$a_5 = -0.10131180E{-}12$$

for temperatures between 1000 and 5000 K. The addition of the subroutine to calculate the local values of the specific heats resulted in less than a 5% increase in CPU time.

Tables 2 and 3 contain time mean of the mass-averaged relative frame flow quantities predicted by the Navier–Stokes simulation and meanline analysis for the constant and variable flow property simulations, respectively. The values presented for the Navier–Stokes simulations were time and mass averaged at the computational inlet (located approximately one axial chord upstream of the vane leading edge), midway between the vane trailing edge and rotor leading edge and at the computational exit (approximately 1.25 axial chord lengths downstream of the rotor trailing edge).

Table 2 Case 1 time-averaged relative reference frame flow quantities

	Navier–Stokes		Meanline	
Variable	Vane	Rotor	Vane	Rotor
M_{in}	0.12	1.15	0.12	1.22
M_{out}	1.42	1.12	1.52	1.30
P_{in}, MPa	15.2	4.20	15.2	3.87
P_{out}, Mpa	4.20	2.89	3.87	2.89
Ht_{in}, kJ/kg	1787	1622	1787	1619
Ht_{out}, kJ/kg	1786	1614	1787	1619
Pt_{in}, MPa	15.4	9.49	15.4	9.44
Pt_{out}, MPa	13.7	6.36	13.8	7.92
β_{in}, deg	0.0	63.7	0.0	72.1
β_{out}, deg	73.3	−61.6	73.8	−70.5
γ	1.354	1.354	1.354	1.354
Reaction	——	0.095	——	0.073
W, kJ/kg	——	284.3	——	285.0
η_{tt}	——	0.608	——	0.635
η_{ts}	——	0.449	——	0.450

Table 3 Case 2 time-averaged relative reference frame flow quantities

	Navier–Stokes		Meanline	
Variable	Vane	Rotor	Vane	Rotor
M_{in}	0.12	1.16	0.12	1.21
M_{out}	1.42	1.10	1.51	1.31
P_{in}, MPa	15.2	4.20	15.2	3.90
P_{out}, Mpa	4.20	2.89	3.90	2.89
Ht_{in}, kJ/kg	1787	1629	1776	1512
Ht_{out}, kJ/kg	1786	1617	1776	1512
Pt_{in}, MPa	15.4	9.36	15.4	9.51
Pt_{out}, MPa	13.4	6.29	13.9	8.05
β_{in}, deg	0.0	63.6	0.0	72.5
β_{out}, deg	73.1	−62.0	74.2	−71.1
γ_{in}	1.363	1.380	1.357	1.383
γ_{out}	1.380	1.381	1.383	1.386
Reaction	——	0.092	——	0.082
W, kJ/kg	——	282.0	——	284.7
η_{tt}	——	0.602	——	0.634
η_{ts}	——	0.447	——	0.450

In general, the results from the Navier–Stokes and meanline analyses display good agreement in the vane passage, but exhibit differences in the rotor passage (see Tables 2 and 3). The meanline analysis predicts more flow turning and higher rotor exit relative Mach numbers, whereas the Navier–Stokes analysis predicts higher losses (associated with the endwall and tip gap flows). The differences between the meanline and Navier–Stokes solutions for the rotor are not surprising because the meanline code relies on empirical

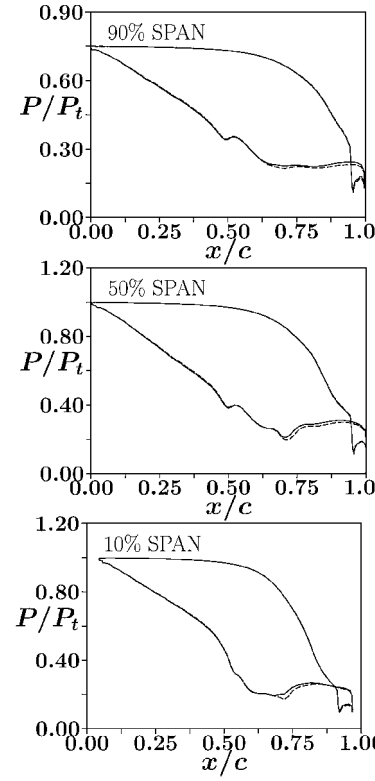

Fig. 2 Time-averaged pressure, vane: ——, case 1 and – – –, case 2.

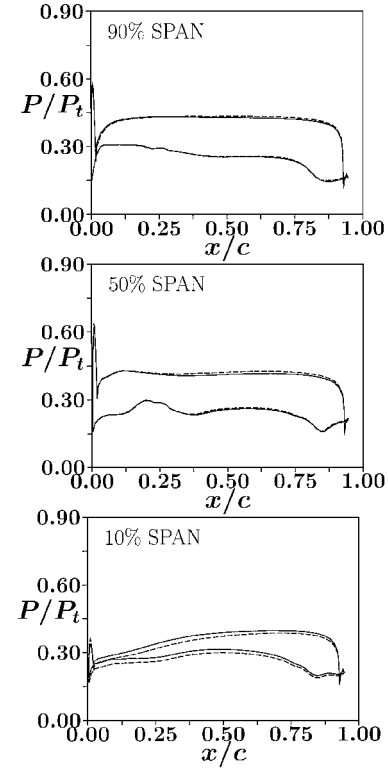

Fig. 3 Time-averaged pressure, rotor: ——, case 1 and – – –, case 2.

loss models for which there are limited data for supersonic turbomachinery flows. The total-to-total efficiencies predicted by the two analyses show fair agreement, whereas the predicted total-to-static efficiencies and work are in excellent agreement.

When the constant and variable fluid property data are compared, the meanline results indicate insignificant changes in both the total-to-total and total-to-static efficiencies, whereas the Navier–Stokes analysis predicts a small decrease in the efficiencies. Both analyses predict a slight decrease in the work extracted by the turbine for variable specific heats.

Time-averaged pressure distributions for the vane and rotor at 10, 50, and 90% span are shown in Figs. 2 and 3, respectively. The vane loadings in both simulations are similar on the pressure surface and upstream of the throat on the suction surface. Downstream of the throat, the case with variable fluid properties displays slightly lower pressures (which agrees with the Mach numbers in Tables 2 and 3) and increased loading. The results from case 2 indicate slightly more loading and higher pressures on the rotor at 50 and 90% span, whereas the loadings are similar at 10% span although the pressures are significantly lower in case 2. The differences at 10% span suggest the nature of the flow in the hub region may be altered by the variable specific heats.

Figures 4 and 5 illustrate a comparison of unsteady pressure traces near the leading edge of the rotor at 10 and 50 span, respectively. Although the pressure traces between 25 and 75% span were similar in both simulations, there were significant differences (in both magnitude and frequency content) at 10 and 90% span, that is, in the endwall regions. Interrogation of the frequency spectrum associated with the unsteadiness at the 10% span location of the rotor (obtained via Fourier decompositions of the unsteady pressure traces) reveals that case 2 contains significantly more unsteadiness at the

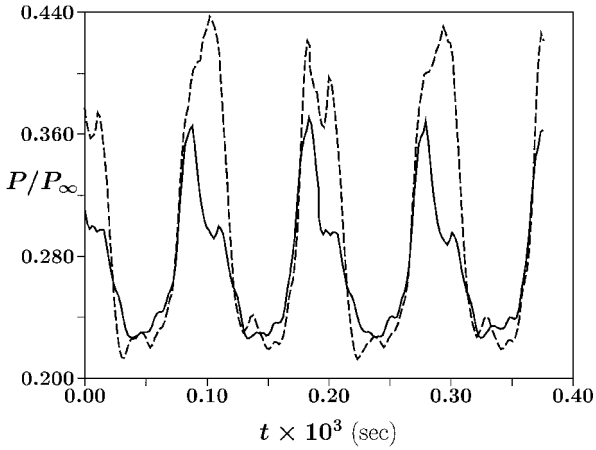

Fig. 4 Pressure history, rotor, 10% span, near leading edge: ——, case 1 and – – –, case 2.

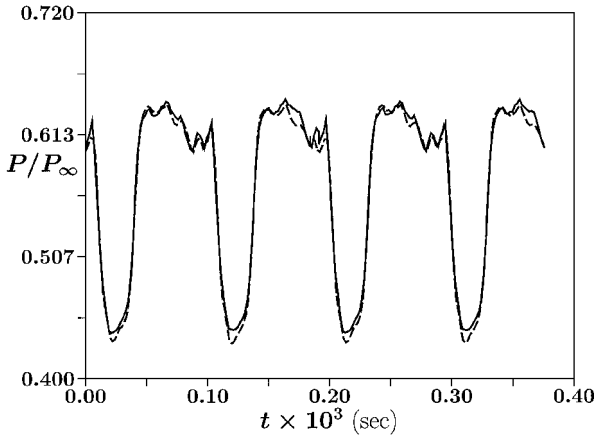

Fig. 5 Pressure history, rotor, 50% span, near leading edge: ——, case 1 and – – –, case 2.

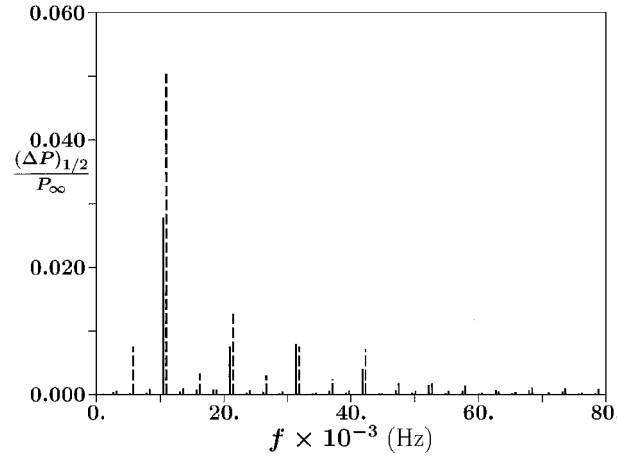

Fig. 6 Pressure decomposition, rotor, 10% span, near leading edge: ——, case 1 and – – –, case 2.

vane passing frequency (approximately 10,000 Hz), as well as increased unsteadiness below and above the vane passing frequency (see Fig. 6). In Fig. 6 the frequencies for case 2 were offset by 500 Hz to facilitate comparisons with case 1. In an effort to determine if the differences in the unsteady pressures at 10% span are confined to the leading edge of the rotor, additional traces were compared on both the suction and pressure surfaces. The traces showed similar behavior to the one near the leading edge. Thus, the unsteady pressures appear to be different in regions normally associated with strong secondary flows.

Conclusions

A set of unsteady three-dimensional Navier–Stokes simulations has been used to investigate the effects of varying specific heats on the performance of a supersonic turbine stage. One simulation was performed assuming constant specific heats, and one was performed in which the specific heats varied locally as a function of the static temperature. The results of both simulations have been compared with the output from meanline simulations.

The flow quantities predicted by the meanline and Navier–Stokes analyses (for both constant and variable flow properties) show good agreement at the exit of the vane, but exhibit significant differences at the rotor exit (which is to be expected because of the lack of data and correlations available for supersonic turbines). There is excellent agreement between the total-to-static efficiencies and work predicted by both analyses.

The Navier–Stokes results indicate increased pressure unsteadiness in the endwall regions for variable specific heats. In addition, the losses increased and the efficiencies decreased in the variable fluid property simulation. The meanline analysis predicted little change in the efficiencies for variable fluid properties, but, similar to the Navier–Stokes results, indicates reduced work. Thus, the current results indicate that it is important to include the effects of variable specific heats.

References

[1] Griffin, L. W., Huber, F. W., and Sharma, O. P., "Performance Improvement Through Indexing of Turbine Airfoils: Part 2: Numerical Simulation," *Journal of Turbomachinery*, Vol. 118, No. 4, 1996, pp. 636–642.

[2] Garcia, R., Griffin, L. W., Benjamin, T. G., Cornelison, J. W., Ruf, J. H., and Williams, R. W., "Computational Fluid Dynamics Analysis in Support of the Simplex Turbopump Design," Vol. 1, NASA CP-3282, 1995, pp. 462–470.

[3] Griffin, L. W., and Dorney, D. J., "Simulations of the Unsteady Flow Through the Fastrac Supersonic Turbine," *Journal of Turbomachinery*, Vol. 122, No. 2, 2000, pp. 225–233.

[4] Dorney, D. J., Griffin, L. W., and Huber, F., "A Study of the Effects of Tip Clearance in a Supersonic Turbine," *Journal of Turbomachinery*, Vol. 122, No. 4, 2000, pp. 674–673.

[5] Wang, T.-S., "Thermophysics Characterization of Kerosene Combustion," *Journal of Thermophysics and Heat Transfer*, Vol. 15, No. 2, 2001, pp. 140–147.